Proceedings of the Institute of Acoustics

HIGH POWER MAGNETOSTRICTIVE TONPILZ TRANSDUCERS

F Claeyssen, N Lhermet, R Le Letty

Société CEDRAT Recherche, ZIRST 4301, F38943 MEYLAN Cedex, FRANCE

1. ABSTRACT

Due to the continuing interest of the French Navy (DCN & DRET), significant improvements have been made to magnetostrictive transducers to produce low-frequency, high-power sonar sources. Much progress has been made in the field of Tonpilz transducers as a result of these improvements. The previous Quadripode transducer was built in two versions, Quadripode I and II. They had acoustic power of 1.0 and 1.6 kW, respectively. Next, an attempt to design a third version of the Quadripode led to a new Tonpilz transducer called the Tripode. Its purpose is to reach an acoustic power of at least 3 kW. It benefits from magnetic circuit design results and from the giant dynamic strain capability of Terfenol-D (Peak-to-Peak strain higher than 2400ppm) discovered in 90-91. In this paper, the modelling results are reminded, and the results obtained from the first series of in-water measurements of the Tripode are analyzed. These results tend to confirm expectations.

2. INTRODUCTION

Rare earth-iron magnetostrictive alloys discovered by A.E.Clark [1] feature 'giant' strains [2] when excited by a magnetic field. Among these materials, Terbium Dysprosium Iron alloy, called Terfenol-D, is the most interesting material because of its high magnetostrain level (typically 1600 ppm). Sonar designers started using this material in the late seventies for low-frequency high-power sonar transducers [3]. French Navy research on this subject started in 1985, with the design of the Quadripode, a Tonpilz type transducer based on four Terfenol-D rods. The first version of this transducer built in 1986 had a 1.0 kW acoustic power [4]. The second version, tested in 1989, had an improved acoustic power, 1.6 kW [5,6] due to the use of Grain-Oriented Terfenol-D.
The discovery of specific properties of Terfenol-D considerably increased interest in its use for magnetostrictive transducers. Under a dynamic state, especially at resonance, the Terfenol-D strain is not limited by the static maximum magnetostrain [6]. For example with appropriate bias and prestress conditions, a dynamic peak-to-peak strain of 2440 ppm in the Terfenol-D was measured in an in-air transducer [7]. In the same manner, strains of 3500 ppm were recently reached [8]. These giant dynamic strains lead to rather large displacements which are of primary importance when building low-frequency high-power transducers. The second interesting property is the very high magnetic limit of the material [6,9] which permits high dynamic strain to be reached not only in a non-loaded transducer but also in very highly loaded transducers. Due to both these properties, magnetostrictive transducers are, theoretically, much more powerful than piezoelectric transducers. These results have led to two areas of research.
The first area of research is related to the drivers. In order to produce the 'giant' strain in sonar transducers, it is necessary to solve the problem of applying the high magnetic bias to Terfenol-D. The chosen method to deal with this problem consists of studying three drivers, that have different magnetic bias systems [8,9,10]. The first driver is biased using a coil. The second driver uses permanent magnets in a parallel configuration. The third driver is biased using permanent magnets in a series configuration. Each type of driver has different properties and aspect ratio. These drivers can now be used as components for the electromechanical energy conversion in any transducer.

The second area of research is related to low-frequency transducers. Three different transducers, a Tonpilz-type, a double-ended vibrator, a class IV Flextensional type are studied [11]. Among these, the new Tonpilz-type, the Tripode, was built. It integrates the experience acquired from the development of the Quadripodes and of the drivers. The first series of in-water measurements was performed in August 1993 by DCN Toulon at Castillon lake. The analysis of the results, done by Cedrat in 1994, included complementary in-air measurements.
The purpose of this paper is to remind the performance expectations, to present the results of the measurements and to comment on the success of the project.

3. DESIGN AND MODELLING RESULTS OF THE TRIPODE

A preliminary study of the Quadripode II transducer was performed by Cedrat in 1991 to determine if giant dynamic strains could be applied to this transducer. The expected advantage was an increase in its acoustic power. Built by DCN in 1987, the Quadripode is a Tonpilz transducer based on four Terfenol-D rods 100 mm in length and 18 mm in diameter. In this transducer, the level of peak-to-peak strain at resonance reached about 1950 ppm leading to an acoustic power of 1.6kW (Table 1) at 1.15kHz. Because the power of a transducer is proportional to the square of the strain in the active material, the use of a 3000ppm strain in the Terfenol-D should lead to a 3.8 kW acoustic power. In principle, such increase of strain could be obtained simply by using higher prestress and excitation levels [7]. In practice, several technological problems must be solved. A higher prestress implies modifying the prestress bolt. A higher excitation implies changing the magnetic circuits (because of larger fluxes), the coils and the cooling device (because of higher dissipated power). Moreover, the use of a higher prestress also implies using a higher magnetic bias [8] to minimize Young's modulus and maximize the coupling coefficient. So the bias magnetic circuit and the bias coil must also be changed. Finally considering all the changes to be made, it was decided to build an entirely new transducer that could be compared to the Quadripode.
This new transducer (Figure 1), designed by Eramer and Cedrat for DCN, is called the Tripode because it is based on three Terfenol-D rods. This choice has been made for obvious mechanical reasons and because the concept of an open magnetic circuit has been proved valid in recent studies of drivers [9,10]. On that point and with the objective of high power, the design is different from a former 3-rod US transducer [3]. Since it was decided to re-employ material already used in the driver study (cylindrical rods of 100mm in length and 20mm in diameter), the total volume of Terfenol-D is 8% smaller than that of the Quadripode. However, in spite of this reduction of active material volume, the stiffness of the transducer remains nearly the same because the diameter of the prestress rod was increased. Its headmass is the same as Quadripode's. It is made of aluminium and its diameter is 287 mm. Its tailmass is also nearly the same as the Quadripode's. So both transducers have almost the same in-water resonant frequency (about 1.2 kHz). The acoustic load of the transducers is also the same. Under these conditions, any increase of acoustic power between the Tripode and the Quadripode can be attributed to an improvement in Terfenol-D strain level .The transducer was designed to gather all the conditions required to get giant dynamic strains and to double the acoustic power to between 3 and 4 kW, in spite of a smaller amount of Terfenol-D.
Models created in 1992 indicated that this power could be achieved (table 1) [11]. Two slightly different sets of Terfenol-D properties have been assumed in modelling in order to see the influence of the material's quality. The first assumption was that the material had a reasonable coupling factor ($k_{33}=63\%$) and reasonable mechanical losses ($Q_m=10.3$). The second assumption was that the material had a high coupling factor ($k_{33}=80\%$) and high mechanical losses ($Q_m=6.7$). The most important result is that the maximum acoustic power does not change.

HIGH POWER MAGNETOSTRICTIVE TONPILZ TRANSDUCERS

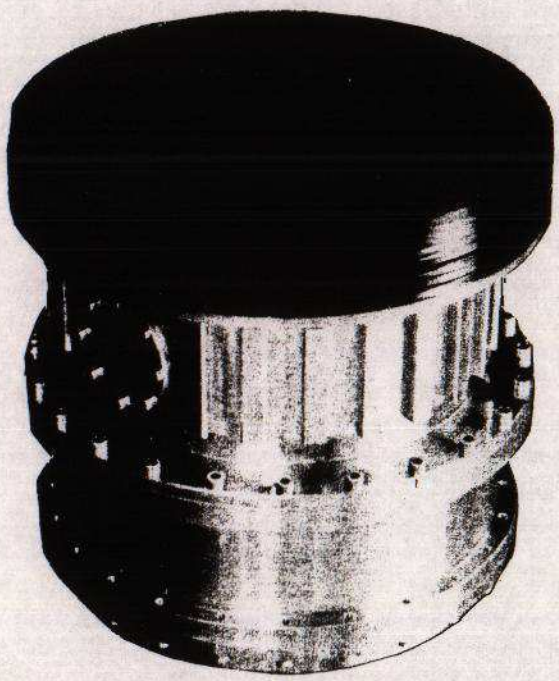

Figure 1 (Right) - View of the Tripode

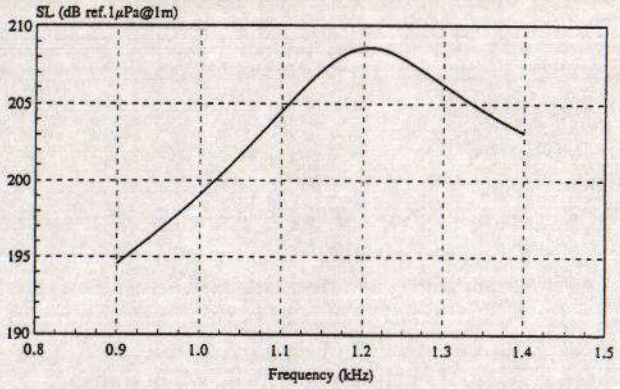

Figure 2 - Tripode Theoretical Source Level
(Ie= 20Arms, Ve= 540 Vrms at resonance)

Name of the transducer		Quadripode	Tripode	
Transducer volume	(dm^3)	51	22	
Active material volume	(dm^3)	0.102	0.094	
Type of data		Measurement (Final results)	Prediction assuming k_{33} = 63%	Prediction assuming k_{33} = 80%
Resonant frequency	(kHz)	1.15	1.20	1.15
Mechanical Q		2.5	6	5
Over voltage factor		2.0	0.7	0.3
Coupling coefficient	(%)	50	50	59
AC-efficiency	(%)	25	45	36
Directivity	(dB)	2.	2.	2.
Transmit.Voltage Resp.	(dB)	142	154.0	153.3
DC power (Bias)	(kW)	2.0	2.3	2.3
Excitation voltage	(V_{rms})	1000	540	590
Active electric power	(kW)	7.2	8.5	11.3
Reactive electric power	(kVA)	15	6.4	3.6
Total efficiency	(%)	17	35	30
Acoustic power	(kW)	1.6	3.8	4.1
Source level	(dB)	205	209	209
Figure of Merit	(J/m^3)	10	24	34

Table 1 - Comparison of two different magnetostrictive Tonpilz transducers
(Measurements of the Quadripode and predictions of the Tripode [11])

This power leads to a source level around 209dB (ref. 1μPa @1m). Figure 2 shows the source level versus frequency at constant excitation current Ie =20Arms. The new transducer also benefits from coil improvements. The excitation coils are different from the bias coils. This permits the electric reactive power and the excitation voltage to be reduced. As a consequence, the excitation voltage Ve required to achieve the maximum source level is only about 550 Vrms at the resonant frequency. So, the expected Transmitting Voltage Response (TVR) is about 154 dB (ref. 1μPa @1m). Modifications to the magnetic circuits, coils and mechanical parts reduced losses and increased efficiency according to theory. A bladder inside the transducer compensates for hydrostatic pressure to a depth of 50 m. An auxiliary high-depth gas compensation device could be added to increase the maximum depth to 300 m. Modifications to the cooling and hydrostatic compensation system led to a reduction in volume by a factor fo 2.5. Thus, the transducer's total length is only 310 mm and its diameter is 300 mm. These performances lead to a potentially high figure of merit (FMV). This figure is defined by the ratio of acoustic power to frequency, the mechanical Q and the transducer volume. It is equivalent to an energy density. Typical values for piezoelectric Tonpilz are about 2J/m3. A 10 times higher value is expected for the Tripode [6].

4. EXPERIMENTAL RESULTS AND ANALYSIS

Tests are still incomplete, but the first series of in-water and in-air experimental results tends to confirm the predicted performance shown in Table 1.
The TVR was measured at Castillon lake by DCN in August 1993 (Figure 3). A rather high excitation level was used (Excitation voltage Ve = 256 Vrms). The measured TVR shows a maximum of 154 dB (ref 1μPa @1m) at a frequency of 1.2 kHz. A 3dB pass band width of 220 Hz leads to a mechanical Quality factor of 5.5. These results are in agreement with expectations.

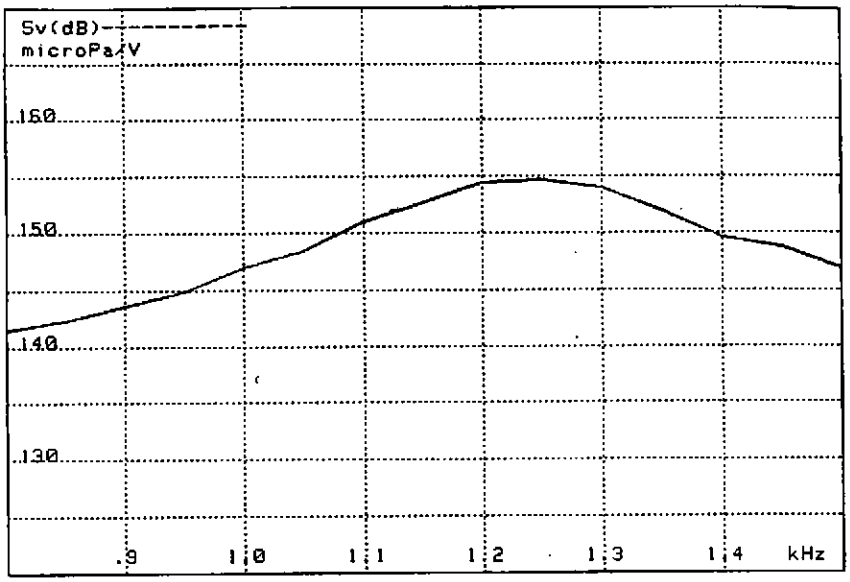

Figure 3 - Tripode measured TVR

The electric impedance was measured at the same time. Surprisingly, it showed a very large difference with theoretical results. This difference has led to further investigations both on the transducer and on the measurement method.

The experimental set-up used for the excitation and the bias of the transducer (Figure 4) has been analysed. The bias circuit is made of the bias coils of the transducer which are driven by a DC power supply through a blocking inductance. This inductance must present a high impedance at the transducer's working frequencies. Its purpose is to allow the DC current for the bias to pass, and to prevent any AC current from coming from the excitation. Due to the magnetic coupling between the bias coils and the excitation coils, the impedance of the bias circuit Zbias is in parallel with the transducer impedance Zt. So the measured impedance Zm is indeed Zbias in parallel with Zt. When the blocking inductance is in good working order, Zbias is high compared to Zt and Zm is almost equal to Zt.

The analysis revealed that the blocking inductance was indeed in short-circuit. This component was probably destroyed by heating during preparation trials. A high rate of AC current exists in the bias circuit when the transducer is excited. Because the impedance of the DC power supply is also very low, Zbias is reduced to the self impedance of the bias coils. In order to characterise Zbias, another measurement of the transducer was performed in air at 1kHz, in two situations. The first measurement was done with the bias coils in open circuit and the second one was done with the bias coils in short circuit. From this, Zbias has been calculated as a resistance Rbias=15,8 Ohm in series with an inductance Lbias= 3.4mH.

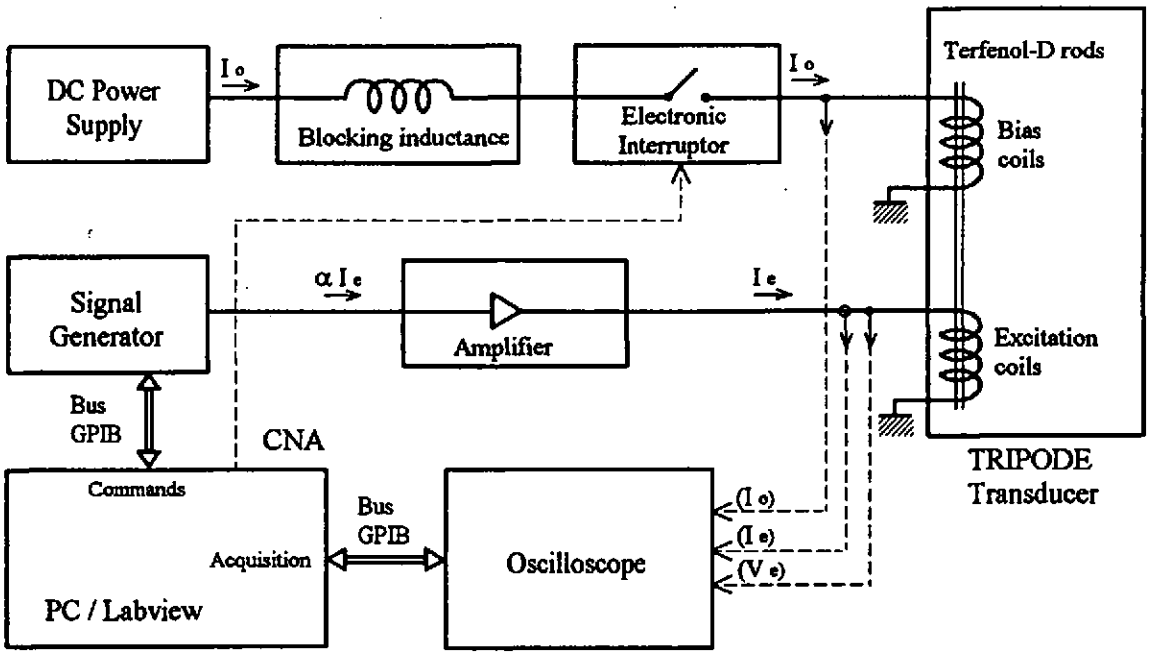

Figure 4 - Set-up used in experiments

Then the impedance of the transducer in water has been recalculated to account for this parallel impedance (Table2). The result is a much greater resistance, in good agreement with predictions that were made with the highest material coupling coefficient. The other transducer parameters were also deduced. As the perturbing impedance is in parallel, the TVR is not modified. Conversely, the Transmitting Current Response (TCR) is significantly changed: The short circuit caused by the failing bias circuit consumes some current. Computations show that half of the input Ampere-turns are consumed by the bias circuit and are unavoidable for magnetomechanical energy conversion. Again, the correction provides a result in much better agreement with the theoretical predictions. Finally, the corrected value for the efficiency is better, which is logical.
It must be noted that the correction produces results which are as good as the best theoretical expectations. So it might be a bit optimistic. A new series of in-water measurements will be performed with a good bias circuit to confirm the expected results.

Type of data		Prediction assuming k_{33} = 63%	Prediction assuming k_{33} = 80%	Experiment without correction	Experiment with correction
Resonant frequency	(kHz)	1.20	1.15	1.20	1.20
Mechanical Q		6	5	5.5	5.5
Series Resistance	(Ohm)	22	28	11	28.7
Series Inductance	(mH)	2.2	1.3	1.5	1.6
Over voltage factor		0.7	0.3	1.0	0.4
Coupling coefficient	(%)	50	59	40	56
Transmit.Voltage Resp.	(dB)	154.0	153.4	154.0	154.0
Transmit.Current Resp.	(dB)	182.8	182.8	178.0	183.9
Directivity	(dB)	2.	2.	2.	2.
AC-efficiency	(%)	45	36	30	45

Table 2 - Comparison of predicted and measured results of the Tripode.
Experimental results are given without and with the correction
related to the failing blocking inductance

5. CONCLUSION

The Tripode magnetostrictive transducer was built in order to check the giant dynamic strain capability of Terfenol-D in a transducer. Modelling results show that such a giant strain is possible and leads to a very high power (between 3 and 4kW) considering its small volume and its frequency.
The first series of in-water measurements showed that the anticipated Transmitting Voltage Response was achieved. Other measured parameters like the electrical impedance and efficiency are also in agreement with the theoretical ones, if a correction related to the failure of the blocked inductance is taken into account. Further in-water trials are required to make more definitive conclusions, especially concerning the power limits of the transducer. Meanwhile, the agreements found between theory and experiments permit us to be reasonably optimistic.
Finally, the experience acquired with the Tripode will be useful for building other high-power transducer projects like a double-ended transducer, for example.

6. ACKNOWLEDGEMENT

The authors would like to thank Mr Boucher, DCN Ingénierie Sud /LSM and Miss Colin, DRET SDR, DGA for their support of this work.

7. BIBLIOGRAPHY

[1] A.E.CLARK, Magnetostrictive rare earth-Fe2 compounds, Ferromagnetic materials, Ed. E.P. Wohlfarth, Amsterdam, North Holland, Tome 1, 1980, pp.531-588.
[2] C.TYREN, Giant magnetostrictive alloys, Proc. of first Int. Conf. on giant magnetostrictive alloys and their impact on actuator & sensor technology. Ed.C.Tyren. Lund(S): Fotynova 1987, pp.215-227
[3] S.W.MEEKS , R.W.TIMME, Rare earth-Iron magnetostrictive underwater sound transducer, JASA, 1977, Vol.62, n°5, pp.1158-1164.
[4] F.CLAEYSSEN, D.BOUCHER, C.POHLENZ, Application of magnetostrictive rare earth-iron alloys to sonar transducers. Proc.UDT88, London, Microwave Exh. & Pub. Ltd, UK, 1988, pp.711-717
[5] F.CLAEYSSEN, Conception et réalisation de transducteurs sonar basse fréquence à base d' alliages magnétostrictifs terres rares - fer, Doctoral thesis, INSA de Lyon (Fr.), 1989, 414 p. *English version available at* Defence Research Information Center (HSMO, MoD, London) *under the name:* Design and building of low-frequency sonar transducers based on Rare Earth Iron magnetostrictive alloys.
[6] F.CLAEYSSEN, D.BOUCHER, Design of Lanthanide magnetostrictive sonar projectors, Proc. UDT91, Microwave Exh. & Pub.Ltd, April 1991, pp.1059-1065
[7] F.CLAEYSSEN, D.COLOMBANI, Giant dynamic magnetostrain in rare earth-iron magnetostrictive materials, IEEE Trans.MAG., Vol.27, Nov.1991, pp.5343-5346
[8] F.CLAEYSSEN, N.LHERMET, R.LE LETTY, State of the Art in the field of Magnetostrictive Actuators, Proc. Actuator 94 conf., Pub. Axon, Bremen (G), 1994, pp. 203-209
[9] M.B.MOFFETT, A.E.CLARK, M.WUN-FUGLE, J.LINDBERG, J.TETER, E.McLAUGHLIN, Characterization of Terfenol-D for magnetostrictive transducers. JASA, Vol.89(3), 1991, pp.1448-1455
[10] F.CLAEYSSEN, N.LHERMET, G.GROSSO, Giant Magnetostrictive Alloy Actuators, Proc Magnetoelastic Effects and Applications Conf., Ed. L.Lanotte, Pub. Elsevier, Holland, 1993, pp.153-160, *also* Int. Journ. of Applied Electromagnetics in Materials, 5 , 1994, pp.67-74
[11] F.CLAEYSSEN, N.LHERMET, J.C.DEBUS, J.N.DECARPIGNY, B.HAMONIC, G.GROSSO, Progress in magnetostrictive sonar transducers, Proc. UDT93, Ed.Reed Exhib., UK, June 1993, pp. 246-250

Proceedings of the Institute of Acoustics

EFFECT OF SHADING ON MULTIHEAD ARRAY BEHAVIOUR

C. BERNARD (1) - D. BOUCHER (1) - P. DUGAST (2)

(1) DCN/ING/SUD - Le Brusc - 83140 Six-Fours les plages- France
(2) SINAPTEC - Parc club des prés - 16 Rue Papin - 59658 Villeneuve d'Ascq - France

ABSTRACT

A transmitter array of sonar transducers called multihead array has been developped as a low-frequency solution with horizontal omnidirectionnal radiation. This array is a stack of four cylindrical rings. Each of them is composed of ten Tonpilz-type transducers mounted in a star-shape around an unique tailmass. Four free-flooded configurations and one with compliant tubes have been built.
At first, numerical modelling using the finite element code ATILA was done to evaluate the acoustical performances. The results are in good agreement with measurements for the different configurations.
The acoustical interactions and the geometry of the array induce some magnitude and phase velocity differences between the rings. In theory, if these differences were controlled, there would be more acoustical power and a better directivity. As an horizontal plane of symmetry exists for the array, the study is limited to two rings, one external and one internal. To modify the difference between the rings, shading of the electrical excitation is applied. The behaviour of the array with such variation is studied. With numerical results it appears that the array has a more complex behaviour that usual rules of thumb show. When the values of shading are adjusted, an increase of the horizontal transmitting voltage response and a decrease of the vertical response are obtained.

I. ARRAY DESCRIPTION

The multihead array has been developed for the new generation of low-frequency emission arrays [1]. This array has an unlimited operating depth. The dimensions and the weight are reduced compared to the previous low-frequency array solutions.

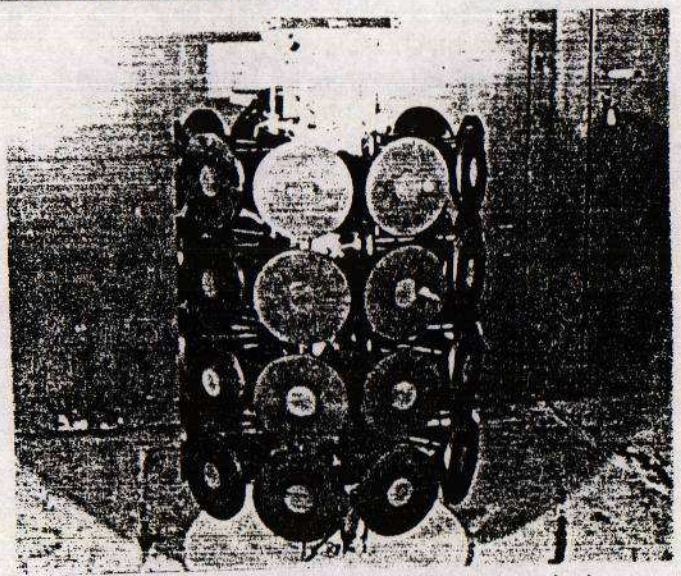

Figure 1 : Multihead array (compact version)

1.1. The rings

The multihead array is a stack of four cylindrical rings. Each of them is 700 millimetres large and 220 millimetres high (figure 1). Each ring is composed of ten Tonpilz-type transducers mounted in a star-shape around a central steel tailmass. Ceramic stacks and circular steel headmasses are surrounded with rubber. The piezoelectric drivers are made up of hard ceramics (Navy III type). The four rings are electrically driven in parallel.

1.2. Description of the different configurations

Five configurations of the array have been built. All of them are free-flooded with no baffle around the structure. The first configuration, referred by compact version, will be studied here. In this version, no space is left between the rings. The second and third configurations are higher : the rings are more separate. In spite of good acoustical performances, these two cases have the disadvantage of being more cumbersome. The fourth configuration developed is the compact one completed with thirty compliant tubes inserted between the pillars. The performances are improved but the structure becomes more complex and expensive. In the fifth configuration, the height of the array is reduced of 90 millimetres by setting off the rings, which overlap the headmasses. For the moment, experimental results didn't reveal great difference between the first configuration and this version, but this solution will be discussed in future studies.

II. ARRAY MODELLING

2.1. Description of the modelling

The finite-element code used to model the multihead array is ATILA (Analyse de Tranducteurs par Intégration des équations de LAplace) developed at Lille by ISEN [2]. This code is specifically adapted to the modelling of sonar transducers, in air and in water. With this code, modal, static and harmonic analyses are possible.

In the case of multihead array, the symmetry is insufficient to use a two-dimensional model, so a three-dimensional mesh is developed. Nevertheless, the presence of different symmetry planes reduces this mesh to only the fortieth part of the array. Finally, only two half-heads are modelled, one external and one internal (figure 2a).

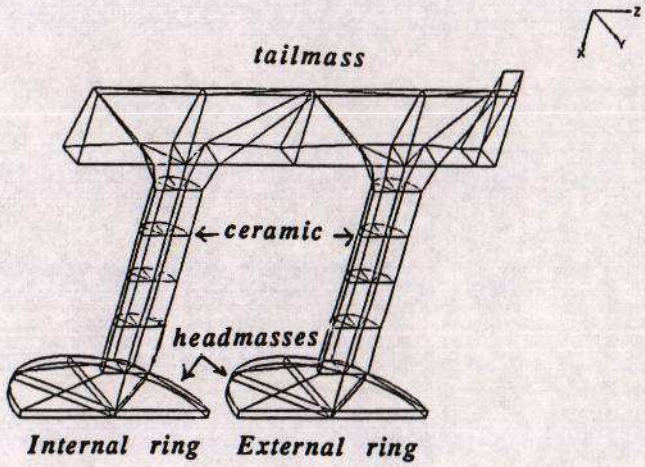

Figure 2a : Modelling of two half-heads (without rubber)

The model includes losses in rubber and in ceramic in the form of complex matrixes.
The fluid inside the array between the tailmass and headmasses is taken into account. To complete the model, the fluid around the array is represented by a spherical domain of sufficient radius (figure 2b). The step of the fluid mesh induces a validity of the results under 2.3 kHz.

In the next paragraphs, transmitting voltage responses at 0 degree and 90 degrees represent respectively the levels obtained face to the centre of each headmass and above the array (figure 2b). They will be designated by TVR (0°) and TVR (90°).

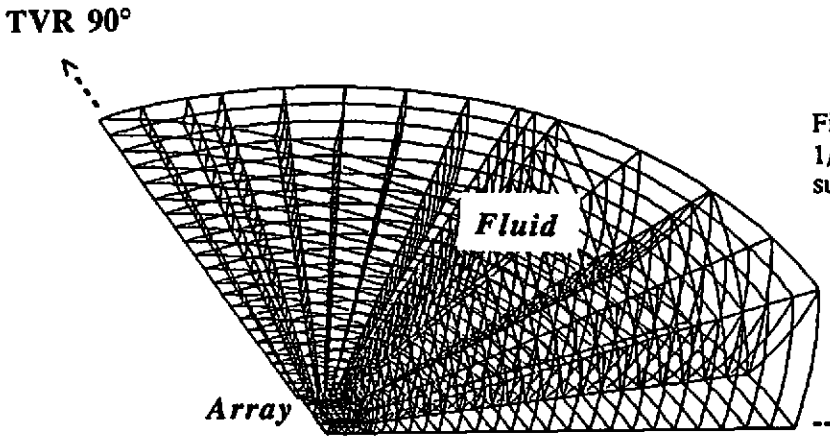

Figure 2b : Modelling of 1/40th of the array with surrounding fluid domain

2.2. Synthesis of the results

In this point, we sum up the results obtained for the first configuration when uniform electrical excitation is applied.

Modal analysis : The modal analysis of the structure reveals several modes under 2.5 kHz. The resonant frequency calculated by ATILA is 1763 Hz, with a coupling factor of 48%. In comparison, the theoretical value obtained with such ceramic is 1807 Hz. This mode depends only on one ring and is not modified in the other configurations.

Harmonic analysis : When the array is dived into water, resonance frequency falls down to 1400 Hz. Figures 3a to 3d present respectively the comparison between numerical and experimental transmitting voltage responses at 0 and 90 degrees, electrical conductance (real part of the admittance), and at last accelerations magnitudes of the two rings. The comparison between numerical results and experience reveals good agreement.

MULTIHEAD ARRAY

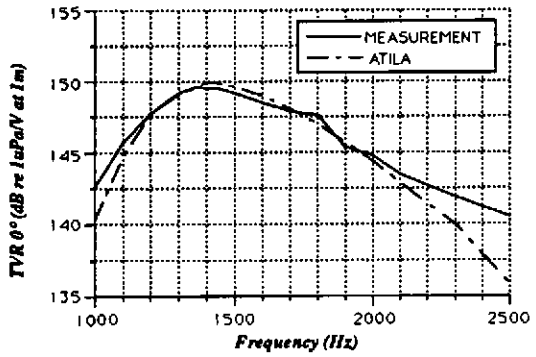

Figure 3a : Transmitting voltage response at 0° (theory and measurement)

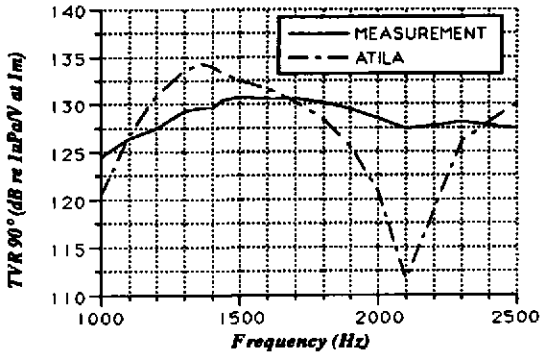

Figure 3b : Transmitting voltage response at 90° (theory and measurement)

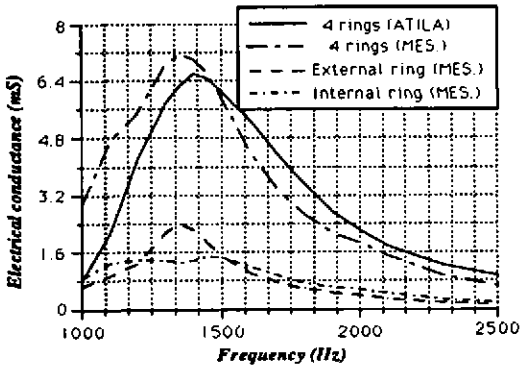

Figure 3c : Electrical conductance - comparison between theory and measurement and comparison between external and internal rings

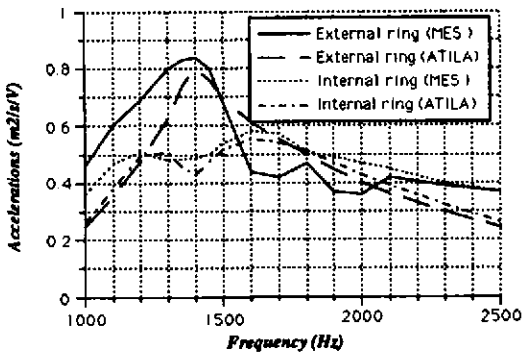

Figure 3d : Accelerations magnitudes of the external and internal rings (measurement and theory)

Maximum transmitting voltage response obtained is 150 dB (ref. 1μPa/V at 1m). The maximum sound level S with a 250 V/mm electric field is calculated by adding 68 dB to the TVR. In our case, S reaches 218 dB. The bandwidth is from 1200 Hz to 1800 Hz. The average electroacoustic efficiency of this array is 50%, and the average directivity index is about 4 dB between 1 and 2 kHz.

Figures 3c and 3d reveal that some difference appears between the external and internal rings. Because of its geometrical position, the external ring works more that the internal one. The other reason of these difference is the reduced space between the headmasses (about $\lambda/5$, where λ is the acoustical wavelength) which leads to acoustical interactions between the rings [1], [3].

The geometrical modifications of the array don't involve great improvement of the performances. For example, the TVR(0°) obtained is 152 dB for the second configuration, whereas the maximum average efficiency is 60% for the array completed with compliant tubes. In the other cases, the difference of behaviour between external and internal rings is not really reduced. A way to optimise the behaviour of this array without changing geometrical structure is now reported.

III. EFFECT OF SHADING ON ARRAY BEHAVIOUR

The results of the last paragraph show that for uniform electrical excitations, the different rings don't have an harmonised behaviour. In any case, the external ring works more that the internal one. That means that a part of the power transmitted is lost, and the behaviour of the array is not optimised. In order to obtain a better harmonisation between the rings, electrical excitations of the two rings can be differentiated in magnitude and phase.

A general study of the array's behaviour depending on the shading applied is developed. First, the study frequency is limited to resonance frequency (1400 Hz). The first point is that the numerical results obtained with ATILA are different from usual basic rules of thumb. Figures 4a shows the variation of magnitudes velocity ratio between internal and external rings when magnitude voltage shading is applied, whereas Figure 4b shows the variation of velocity phase difference when the voltages are dephased.
At resonance frequency, there should be in theory proportionality between the magnitudes and no difference in phase (according to the equation obtained from the electro-mechanical analogy model [4]). As shown in figures 4a and 4b, these two conditions are not observed, hence the rings are coupled via water.

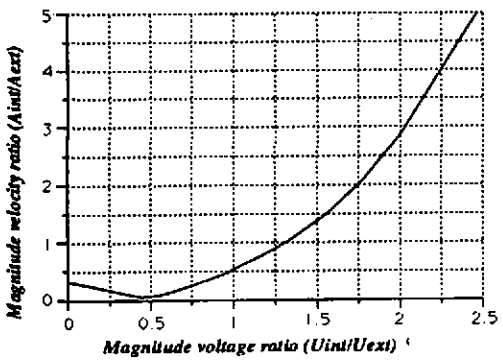

Figure 4a : Variation of magnitude velocity ratio (A_{int}/A_{ext}) versus magnitude voltage ratio (U_{int}/U_{ext})

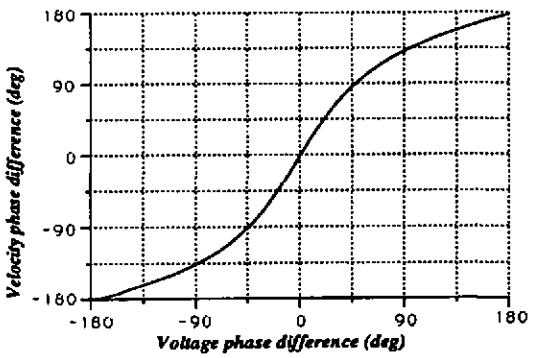

Figure 4b : Variation of velocity phase difference ($\phi_{int}-\phi_{ext}$) versus voltage phase difference ($\phi_{int}-\phi_{ext}$)

Phase shading

When the excitations are dephased, the directivity pattern is principally modified. Figures 5a and 5b show the effect of phase shading on the transmitting level response at zero and ninety degrees, and on the accelerations magnitudes. Figure 5c represents the directivity patterns obtained in three cases of phase difference. All the curves have been obtained at 1400 Hz.

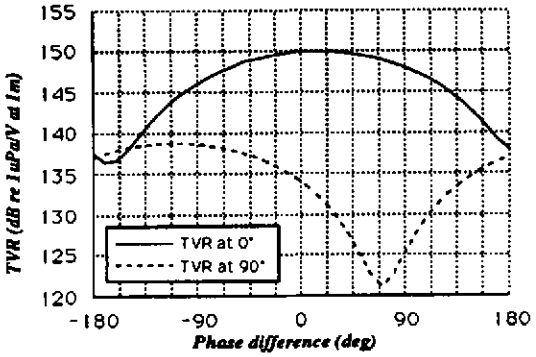

Figure 5a : Variation of the transmitting voltage response versus voltage phase difference ($\phi_{int} - \phi_{ext}$)

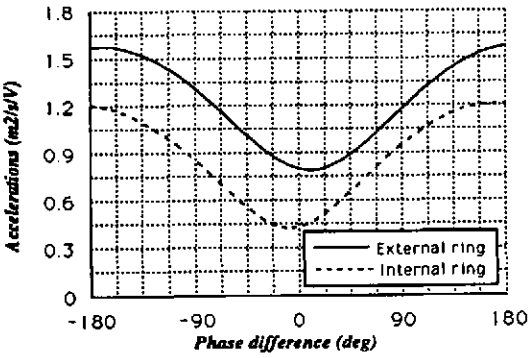

Figure 5b : Variation of accelerations magnitudes versus voltage phase shift ($\phi_{int} - \phi_{ext}$)

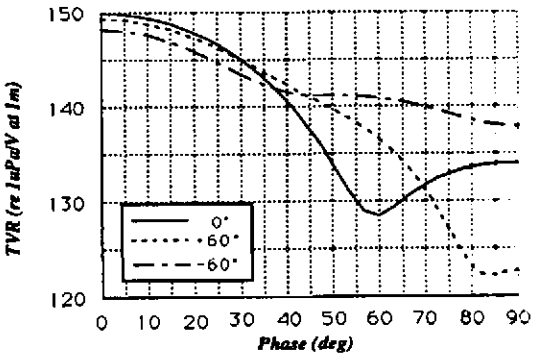

Figure 5c : Directivity patterns for three cases of voltage phase difference ($\phi_{int} - \phi_{ext}$) : -60°, 0° and 60°

First, phase shading has significant influence on the transmitting level. The TVR(0°) keeps a sufficient value (greater than 149 dB) when the phase difference applied is between -40° and 60°. Out of this range, the phase difference is too important to obtain a good transmission of the excitations, then the signal rapidly decreases. TVR(0°) is nearly symmetrical about 0 degrees. It agrees with the theoretical pattern function at 0° in which the phases of the two external or of the two internal rings are conjugated [4]. The small dissymmetry is due to the phase difference that exists initially with uniform excitation.

This symmetry disappears for the TVR(90°). When the phase of the external ring is greater than the internal one, the response increases. On the contrary, when it is lower, the TVR(90°) is consequently reduced (more than 10 dB between 50° and 90°). In fact, phase shading modifies the directivity pattern plot (figure 5c). For a positive increase of the phase difference, the first zero's position of the pattern is set off, and reaches 90° in the zone where the TVR(90°) is minimum.
Figure 5b shows that the velocities magnitudes difference between the rings is reduced in this area.
Relating to the other acoustical results, the variation of efficiency depending on phase shading follows the TVR (0°) variation : it exceeds 40% when the phase is less than 50°. The directivity index has also the same behaviour and becomes useless for important phase differences. At last, the electrical impedance is reduced with phase shift, essentially the conductance.

In conclusion, a positive phase difference (ϕ_{int} - ϕ_{ext}) less than 70° can be useful in terms of level : the TVR (0°) doesn't decrease, whereas the TVR (90°) is lowered. Moreover, the difference between the velocities magnitudes is reduced : the ratio is greater than 70% in this case, whereas the other performances don't really change.

When the same simulation is done for other frequencies (between 1200 and 1800 Hz), the results change in proportion as the frequency differs from the studied frequency. The same general study should be necessary for each frequency.

Magnitude shading

The behaviour of the array depending on magnitude shading is illustrated figure 6a for the transmitting voltage responses at zero and ninety degrees, figure 6b for the directivity index and figure 6c for the accelerations magnitudes. For the excitations, the limit of 250 V/mm is always respected. The frequency is still 1400 Hz.

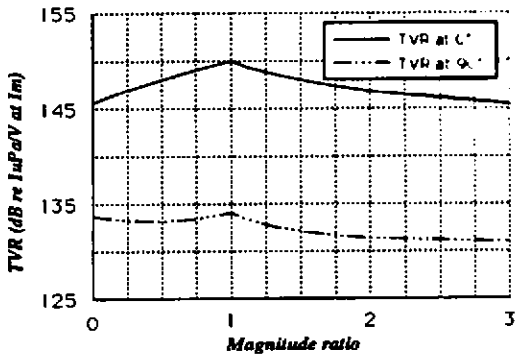

Figure 6a : Transmitting voltage responses at 0° and 90° versus voltage magnitude shading (U_{int}/U_{ext})

MULTIHEAD ARRAY

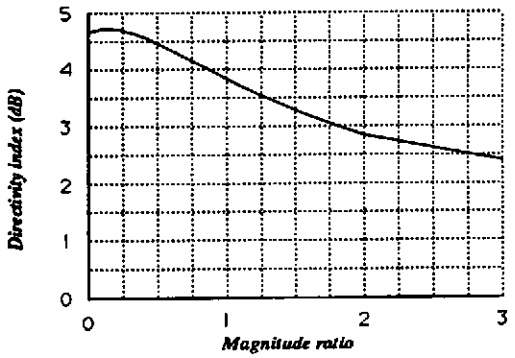

Figure 6b : Directivity index versus voltage magnitude shading (U_{int}/U_{ext})

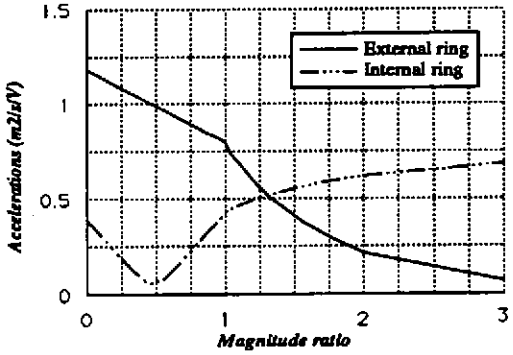

Figure 6c : Accelerations magnitudes of the internal and external rings versus voltage magnitude shading (U_{int}/U_{ext})

Magnitude shading corresponds to a partial excitation of one ring compared to the other one. If we consider a partial excitation of the internal ring, this is not of great interest, except for the directivity [5]. With such shading, the array's radiation is more dipolar, and the directivity index can be improved of about 1 dB when the voltage magnitude ratio is 0.1. But the decrease of the TVR (0°) associated with this shading is 3 dB, and the internal rings are not used in this case (their velocities are closed to zero).

If we take into account the mutual impedances between the rings, the equations associated with the two rings are [6] : $V_{ext} = Y_{11} E_{ext} + Y_{12} E_{int}$

$$V_{int} = Y_{21} E_{ext} + Y_{22} E_{int}$$

where : V_{ext} and V_{int} are the external and internal velocities
E_{ext} and E_{int} are the external and internal voltages
The admittances Y_{11}, Y_{12}, Y_{21} and Y_{22} depend on constants from electrical equivalent circuit.

Hence, the velocity of one ring is a linear combination of the external and internal excitations. For a given ratio of excitations, one velocity can be cancelled. Here, when the ratio is equal to 0.5, the internal ring is nearly motionless.
Following this, a partial excitation of the external ring should lead to a more uniform behaviour of the array (in the case of uniform excitation, the external ring works more that the internal one). As shown in figure 6c, the equality between velocities magnitudes happens when the ratio between internal and external ring is equal to 1.3. For this ratio, the efficiency increases of 5%, but the transmitting level at 0° decreases of 1.4 dB. A way to avoid this decrease is explained in the next paragraph.

A very high or a very low shading ratio is irrelevant because it corresponds to an array of only two rings and so totally changes its behaviour.

MULTIHEAD ARRAY

Magnitude shading with equalisation of the stresses

In the previous sections, shading was applied with respect to the maximum voltage of 250 V/mm. But relating to the maximum level, such shading is not the best solution : the parameter which limits the power is the electric field. Consequently, the TVR(0°) and so the total sound level S quickly decreases when one of the two rings is partly excited (figure 6a).

To prevent from this decrease, the stress can be kept constant instead of the voltage [7]. The constant stress is fixed by the prestress which is 18 MPa in longitudinal motion. The voltages are variable, but another condition fixes their maximum level to 450 V/mm. The optimisation consists in differentiate the excitations in order to equalise the stresses in the two rings. The optimised value of shading between the two excitations is calculated for each frequency in this case.

Figure 7a represents the sound levels S obtained with uniform excitations (400 V/mm) and with optimised excitations. This sound level is obtained with a voltage ratio Uint/Uext = 1.22 and with nearly equal stresses in the two rings. These conditions correspond to the maximum sound level which can be obtained, especially at resonance frequency.

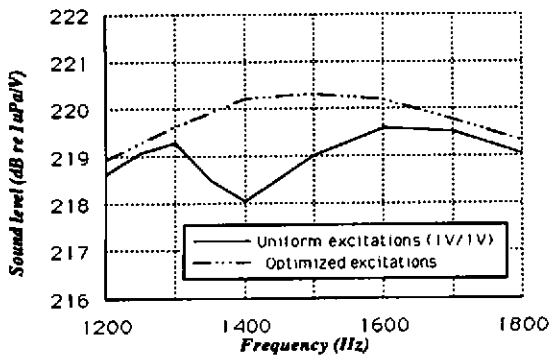

Figure 7a : Comparison of the sound level at 0° with uniform excitation (400 V/mm) and with optimised excitations

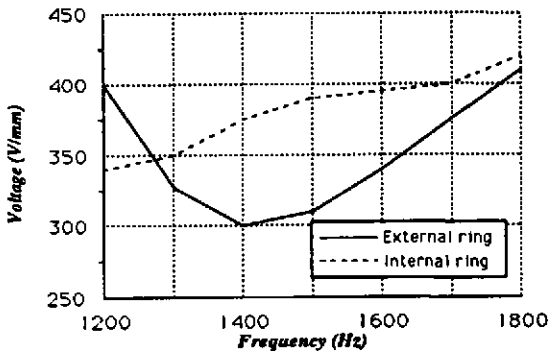

Figure 7b : Variation of the applied voltages corresponding to the optimised excitations

When the optimised ratio is applied, the sound level is increased of 2 dB at resonance frequency. Unfortunately, it's done with an increase of the voltage applied (figure 7b). However, a modification of the ceramic can improve the situation. For ceramic of another Navy III type, the stress increases (30 MPa). In this case, S is greater than 221 dB.

CONCLUSION

This study shows that a good adjustment of magnitude and phase shading between the rings of the multihead array can improve the performances. The principal difficulty is the experimental way of shading (the shading values can't be preliminary determined). An optimisation for each frequency has to be done. Nevertheless, the differentiation of the excitations is useful in different cases : concerning the directivity, a modification of the directivity function is obtained by phase shading (the phase difference value depends on the wanted function), whereas an improvement of the index is obtained with a magnitude shading in which the ratio is less than 0.5. A better harmonisation between internal and external accelerations magnitudes is obtained with a phase shading of about 50° or with a magnitude shading corresponding to a ratio of 1.3 - 1.4. At last, the sound level is improved with an harmonisation of the stresses using magnitude shading.

REFERENCES

[1] DECARPIGNY J.N. & HAMONIC B. & WILSON O.B., 'The design of low-frequency underwater acoustic projectors : Present status and future trends', *IEEE Journal of Oceanic Engineering, Vol. 16, number 1, January 1991*

[2] DECARPIGNY J.N. & HAMONIC B., 'General introduction to ATILA', *Proceedings of the workshop, Toulon, France, 1990*

[3] RICHARDS R.T. & BLOTMAN J.B. (III) & Mc TAGGART B., 'Physics of array element interaction phenomena', *Proceedings Int. workshop, Toulon, France, June 1990*

[4] WILSON O.B., 'An introduction to the theory and design of sonar transducers', *U.S. Gov. Printing Office, Washington, DC, June 1985 (supp. Nav. Sea Systems command)*

[5] AUDOLY C., 'Some aspects of acoustic interactions in sonar transducer arrays', *JASA vol. 89, number 3, March 1991, pp. 1428 - 1433*

[6] PRITCHARD R.L., 'Maximum directivity index of a linear point array', *JASA vol. 26, number 6, November 1954, pp. 1034 - 1039*

[7] DUGAST P., 'Antenne multitête cylindrique - Modélisation et optimisation', *Note technique - Marché AT Junior M91 762448 - Avril 1994 - Sinaptec France*

Proceedings of the Institute of Acoustics

GENERAL SHADING TECHNIQUE FOR SONAR TRANSDUCER ARRAYS

P F Dobbins (1) and G J Heald (2)

(1) BAeSEMA, Marine Division, PO Box 5, Filton, Bristol BS12 7QW
(2) DRA, Southwell, Portland, Dorset DT5 2JS

1. INTRODUCTION

The problem of finding shading coefficients to control transducer array beampatterns grows in difficulty with the complexity of the array and the incompatibility of the directivity requirements. The easiest cases such as the uniform line array require only simple formulae, ranging from the crudest Hann and Hamming functions to the more sophisticated Dolph-Chebychev and Taylor shading schemes, but more perverse situations, conformal arrays for example, call for computer intensive optimisation routines. Many such routines have been described, but most have been restricted to line arrays ([1] is a recent example) or have imposed various uniformity and symmetry constraints (eg [2]).

Optimisation methods aim to find beampatterns that maximise parameters such as the signal-to noise-ratio, but in many practical applications the required beampattern can be specified simply in terms of beamwidth and sidelobe level. In principle, the array response can then be defined at a number of points in space and the resulting equations solved to find the required shading coefficients. This method carries no restrictions on geometry, but requires that the desired pattern be known exactly at a defined number of points; small errors in the specification can lead to large errors in the result or failure to solve the equations.

An alternative is to use the least-squares method, or some other approximation technique, to find weightings that best fit the beampattern equations to the requirements specified at a discrete but arbitrary number of points. Such an approach has previously been demonstrated successfully by the present authors for both line arrays [3] and plane arrays [4]. In this paper, results are presented for three-dimensional array configurations and it is confirmed that, for any arbitrary array geometry, the method can find (possibly complex) shadings to produce any physically realisable beampattern. The method requires little effort to implement on a small computer and the results are easily checked.

2. THE METHOD

The theory and mathematical formulation of the least-squares array shading algorithm were explained in detail in [3] for line arrays. The extension to a completely general 3-dimensional geometry is straightforward, as follows:

GENERAL SHADING TECHNIQUE FOR SONAR TRANSDUCER ARRAYS

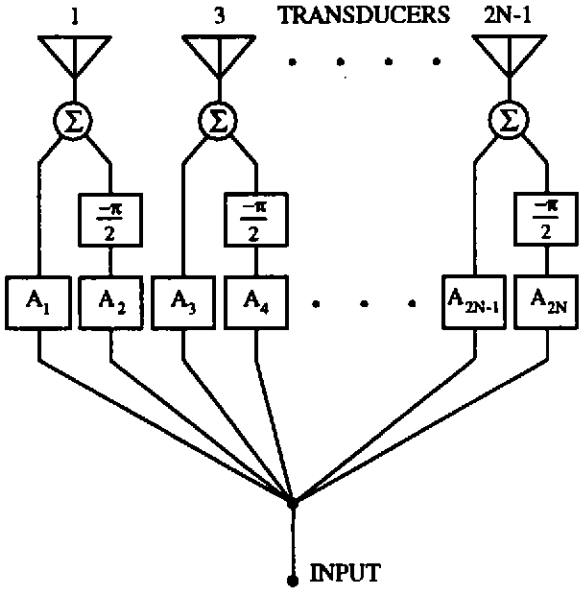

Fig.1 Beamformer architecture.

Consider the completely general beamformer architecture shown in Figure 1. There are N transducers arbitrarily located in space and the signal is split into a separate channel for each transducer. Each of these channels is further split into two channels, one of which is phase shifted by 90° so that the co-phase and quadrature components of the shading coefficients A_n may be applied separately. The outputs from each co-phase/quadrature pair are then recombined and passed to the transducers.

This structure allows the real and imaginary parts of the shading coefficients to be separated, which is convenient for the mathematical formalism, but in practice the results may be expressed in terms of amplitude and phase, or equivalent time delay, and used with a more conventional beamformer. It may be noted that if the array can be represented as pairs of elements symmetrically spaced about the origin, as is often the case in practice, all the arithmetic becomes real and this complicated structure is unnecessary. However, it is the completely general case that is dealt with here. Note also that although a transmitting array is described here, the method may equally be applied to receiving arrays.

Figure 2 shows the nth transducer, with a directivity function $G(\theta,\phi)$, located at an arbitrary point (x_n, y_n, z_n) in Cartesian coordinates. The observation point is in the far field in a direction (θ,ϕ) where θ is the angle of incidence measured from the forward z axis and ϕ is the angle measured from the x axis, in the x,y plane. If z is taken as the polar direction, θ and ϕ are respectively elevation and azimuth.

The sound pressure $P(\theta)$ due to this single element, relative to an imaginary reference element at the origin, is given by

$$P(\theta,\phi) = G(\theta,\phi)\exp\{i(\omega t + u)\} \qquad (1)$$

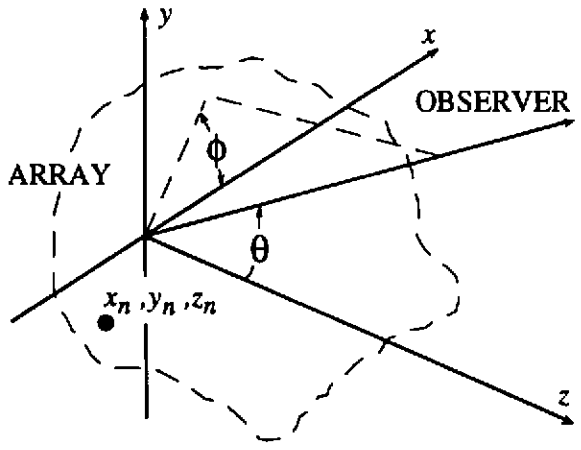

Fig.2 Geometry and coordinate system.

which may be expanded to give

$$P(\theta,\phi) = G(\theta,\phi)\exp(i\omega t)(\cos u + i\sin u) \tag{2}$$

where ω is frequency and u is dependent upon the particular geometry and coordinate system. For example, with the coordinates described and a line array lying along the x axis, u is given by

$$u = kx\sin\theta\cos\phi \tag{3}$$

where $k = \omega / c$ is the wavenumber and c is the speed of sound. In the case of a planar array lying in the xy plane, the relevant form for u is

$$u = k\sin\theta[x\cos\phi + y\sin\phi] \tag{4}$$

and in the general 3-dimensional case, u becomes

$$u = k[x\sin\theta\cos\phi + y\sin\theta\sin\phi + z\cos\theta] \tag{5}$$

These expressions may be further modified to include the effect of beam steering.

The $\exp(i\omega t)$ time dependence may now be dropped, and the output from the array of N such transducers determined by representing each transducer as a pair of identical elements, co-located in space, one driven by the co-phase channel and the other by the quadrature channel. If the weighting coefficients are $A_1, A_2, \ldots, A_{2N}$, the total output is

$$P_{tot}(\theta,\phi) = \sum_{n=1}^{2N} G_n(\theta,\phi)A_n[\cos u_n + i\sin u_n] \tag{6}$$

The transducer position coordinates and directivity functions must be duplicated for each pair of odd and even n's to correspond with the beamformer architecture, so

$$G_n(\theta,\phi) = G_{n-1}(\theta,\phi) \qquad \text{for even } n \tag{7}$$

and

$$u_n(\theta,\phi) = \begin{cases} k[x_n\sin\theta\cos\phi + y_n\sin\theta\sin\phi + z_n\cos\theta] & ;n \text{ odd} \\ u_{n-1} - \pi/2 & ;n \text{ even} \end{cases} \tag{8}$$

The array output, expressed as the right hand side of Eq.(6), may be separated into its real and imaginary parts and each equated to the corresponding real and imaginary parts of the desired response, $D(\theta,\phi)$, at M combinations of θ and ϕ (and possibly ω). A system of linear equations

results which may be solved for the shading coefficients A_n if $M = N$ precisely, but generally, of course, M and N are different. The set of linear equations is

$$\begin{aligned} &A_1 v_{1,1} + A_2 v_{1,2} + \ldots + A_{2N} v_{1,2N} = w_1 \\ &A_1 v_{2,1} + A_2 v_{2,2} + \ldots + A_{2N} v_{2,2N} = w_2 \\ &\quad\vdots \\ &A_1 v_{2M,1} + A_2 v_{2M,2} + \ldots + A_{2N} v_{2M,2N} = w_{2M} \end{aligned} \tag{9}$$

$$v_{m,n} = \begin{cases} G_n(\theta_m, \phi_m)\cos u_n(\theta_m, \phi_m) & ; m \text{ odd} \\ G_n(\theta_m, \phi_m)\sin u_n(\theta_m, \phi_m) & ; m \text{ even} \end{cases} \tag{10}$$

$$w_m = \begin{cases} \mathrm{Re}\{D(\theta_m, \phi_m\} & ; m \text{ odd} \\ \mathrm{Im}\{D(\theta_m, \phi_m\} & ; m \text{ even} \end{cases} \tag{11}$$

where, as with the G_n, the combinations of θ and ϕ have been duplicated, and for even m $\theta_m = \theta_{m-1}$ and $\phi_m = \phi_{m-1}$.

The best approximation to the shading coefficients A_n in the least-squares sense (see eg [5]) may be found by defining a set of vectors, $\vec{V}_n$, formed from the simultaneous equation matrix (Eq.(9)):

$$\begin{aligned} &\vec{V}_1 = (v_{1,1}, v_{2,1}, \ldots, v_{2M,1}) \\ &\vec{V}_2 = (v_{1,2}, v_{2,2}, \ldots, v_{2M,2}) \\ &\quad\vdots \\ &\vec{V}_{2N} = (v_{1,2N}, v_{2,2N}, \ldots, v_{2M,2N}) \end{aligned} \tag{12}$$

$$\vec{W} = (w_1, w_2, \ldots, w_{2M})$$

The shading coefficients are determined from the orthogonality relationships [5]

$$\{(A_1\vec{V}_1 + A_2\vec{V}_2 + \ldots + A_{2N}\vec{V}_{2N}) - \vec{W}\} \cdot \vec{V}_n = \vec{0} \tag{13}$$

which yield a system of $2N$ equations in the $2N$ unknowns:

$$
\begin{aligned}
&(\vec{V}_1 \cdot \vec{V}_1)A_1 + (\vec{V}_1 \cdot \vec{V}_2)A_2 + \ldots + (\vec{V}_1 \cdot \vec{V}_{2N})A_{2N} = \vec{V}_1 \cdot \vec{W} \\
&(\vec{V}_2 \cdot \vec{V}_1)A_1 + (\vec{V}_2 \cdot \vec{V}_2)A_2 + \ldots + (\vec{V}_2 \cdot \vec{V}_{2N})A_{2N} = \vec{V}_2 \cdot \vec{W} \\
&\quad\vdots \\
&(\vec{V}_{2N} \cdot \vec{V}_1)A_1 + (\vec{V}_{2N} \cdot \vec{V}_2)A_2 + \ldots + (\vec{V}_{2N} \cdot \vec{V}_{2N})A_{2N} = \vec{V}_{2N} \cdot \vec{W}
\end{aligned}
\qquad (14)
$$

These are the normal equations for the approximation and may be solved, for example, by straightforward elimination or matrix inversion. This method, as described, will successfully find shading coefficients for line arrays or 2-dimensional arrays that lie in the same plane as the observation point [3]. With a multi-dimensional array lying outside this plane the matrix representing the set of equations (14) may become singular, depending on the symmetries in the array geometry and the desired beampattern. This problem can be overcome either by additional terms in the array response definition Eq.(11) to force similar symmetry in the shading coefficients [4], or by using singular value decomposition methods (see eg. [5]).

3. SOME EXAMPLES

The application of the algorithm to 3-dimensional arrays may be demonstrated with two simple examples. In [4] results were presented for a planar array described in [6] and sketched in Figure 3. A beampattern obtained with this array is shown in a 3-dimensional representation having a vertical range of 50dB in Figure 4. The pattern was computed at a frequency corresponding to an inter-element spacing of 0.7λ, and with shading coefficients giving an

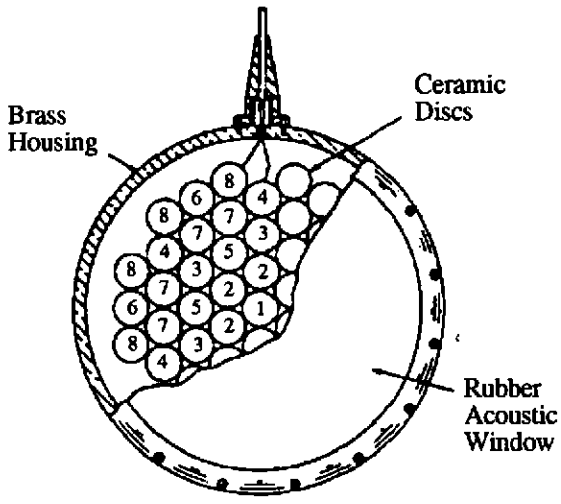

Fig.3 Sketch of USRD F27A array (from [6]).

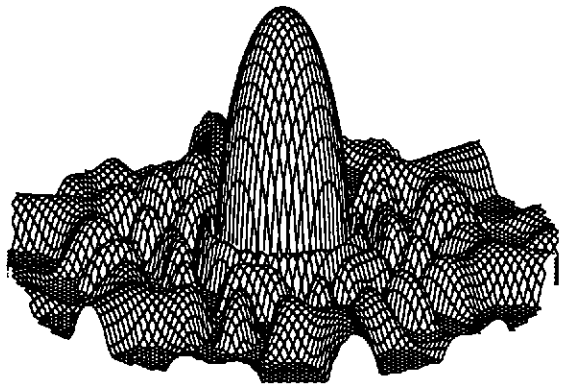

Fig.4 3D representation of F27A beampattern with shading for -41dB uniform sidelobes.

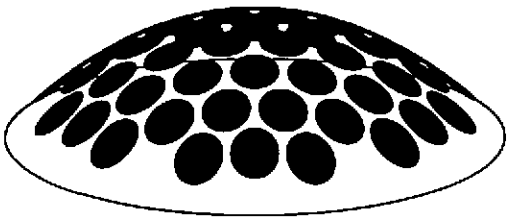

Fig.5 Sketch of F27A array projected on to a spherical surface.

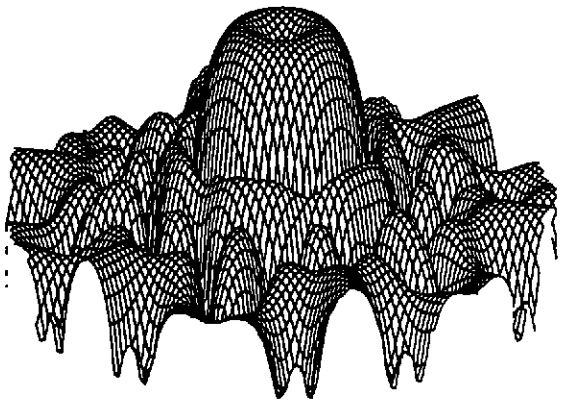

Fig.6 3D representation of spherical array beampattern with original shading coefficients.

approximately uniform -41dB sidelobe level with omnidirectional transducer elements. For the first example, the elements of this array were projected on to a spherical surface with a maximum deviation from a flat plane of $\lambda/2$, as shown schematically in Figure 5. The beampattern obtained with this array and the original shading coefficients, seen from the convex side, is shown in Figure 6. Clearly the curvature introduced into the array geometry has degraded the directivity - the main beam has broadened, with a depression in the centre, and the sidelobe levels have increased.

In order to find new shading coefficients to reduce this degradation, the peaks of the sidelobes in the pattern shown in Figure 4 were located. Their angular coordinates with a nominal level of -41dB were used as inputs to the least-squares algorithm as $D(\theta,\phi)$ in Eq.(11). The resulting beampattern is shown in Figure 7, where it is seen that the shape of the main beam and sidelobe level of the plane array pattern have been restored.

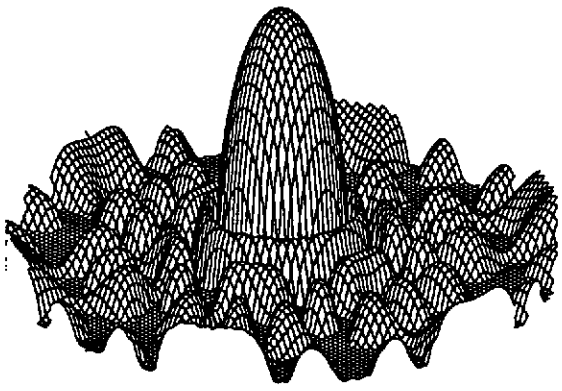

Fig.7 3D representation of spherical array beampattern with least-squares shading coefficients.

For a second example, the array elements were projected on to a surface having a sinusoidal curve in one dimension with a maximum deviation from a flat plane of $\lambda/5$, and shown schematically in Figure 8. The beampattern obtained with this array and the original shading is shown in Figure 9. It is again clear that the curvature has seriously degraded the beampattern. In this

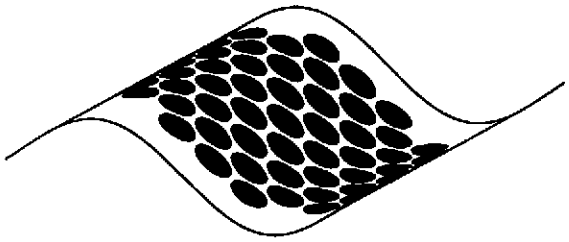

Fig.8 Sketch of F27A array projected on to a sinusoidal surface.

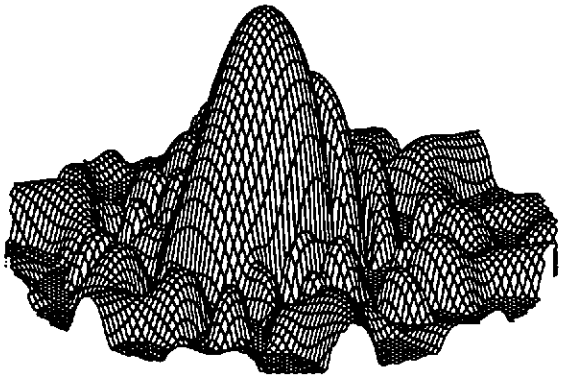

Fig.9 3D representation of sinusoidal array beampattern with original shading coefficients.

case the main beam has split into three peaks and the circular symmetry associated with the hexagonal geometry has been lost.

The data used as inputs to the least-squares algorithm to produce the beampattern shown in Figure 7 were again applied with the new array geometry, and the beampattern obtained is shown in Figure 10. The main beam shape has once more been restored, but the sidelobes have adopted a new distribution and their level appears to have risen. Figure 11, however, is a conventional plot of array response against bearing in elevation at an azimuth corresponding to the highest sidelobes, and shows that the maximum sidelobe level is still -35dB.

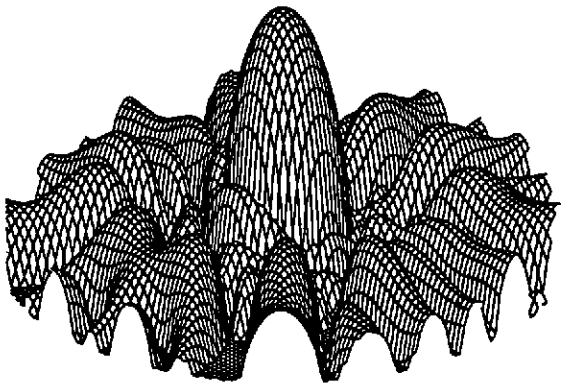

Fig.10 3D representation of sinusoidal array beampattern with least-squares shading coefficients.

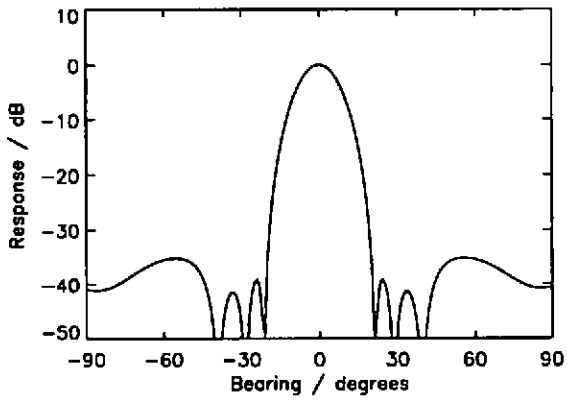

Fig.11 2D plot of sinusoidal array beampattern with least-squares shading coefficients.

Array	DI / dB	Maximum Sidelobe / dB	Beamwidth / deg Azimuth = 0°	Azimuth = 90°
Plane	22.5	-40.7	14.6	14.6
Spherical	22.6	-37.8	14.6	14.6
Sinusoidal	22.8	-35.3	14.1	13.9

Table 1. Performance parameters for plane, spherical and sinusoidal arrays.

The DI, the peak sidelobe level, and the beamwidths measured at azimuth angles of 0° and 90° for each of the three arrays are listed in Table 1, and it is clear that their overall performance characteristics are very similar. It is worth noting at this point that the results presented here were obtained with a single application of the least-squares algorithm using a small selection of data points from the plane array as a definition of the required directivity. There was no attempt at further iteration or optimisation.

The actual shading coefficients produced are listed in Table 2. Presented here are the (real) coefficients of the plane array pattern, the complex coefficients for the spherical array expressed as magnitude and phase, and the magnitude only for the sinusoidal array. Because of the symmetry of the planar and spherical array geometries, as well as the beampattern requirements,

	Plane	Sphere Magnitude	Sphere Phase / deg	z / deg	Sinusoid Magnitude
1	1.0000	1.0000	143.10	144.00	1.0000
2	0.8204	0.8041	131.70	132.41	0.7842
3	0.5008	0.4669	98.18	98.17	0.5106
4	0.1957	0.1731	43.40	42.80	0.2061
5	0.5994	0.5666	109.15	109.51	0.6027
6	0.0779	0.0708	11.83	10.58	0.0881
7	0.2790	0.2491	65.34	64.69	0.2994
8	0.0676	0.0653	3.12	0.00	0.1045

Table 2. Shading coefficients for plane, spherical and sinusoidal arrays.

all elements at the same distance from the array centre have the same coefficients and only eight different values are required, as seen in Figure 3. Because the sinusoidal array does not have this symmetry in the z direction it is found that the magnitudes of the coefficients are grouped in the same way, but not the phases. Also given are the z-coordinates of the spherical array elements in terms of an equivalent phase angle.

It is apparent from Table 2 that the algorithm has found coefficients for the spherical array with phase shifts approximately equivalent to the delays between the element locations and the $z = 0$ plane, combined with magnitudes close to the corresponding plane array coefficients. In the case of the sinusoidal array, the magnitudes remain similarly close to those for the plane array and if space had been available to list all 55 coefficients it would have been seen that the phases were again roughly equivalent to the z-coordinates.

4. DISCUSSION AND CONCLUSIONS

The examples presented here show that, for straightforward cases at least, it is possible to find shading coefficients to produce some previously defined beampattern from a given 3-dimensional array. The only known constraint is that the required directivity be physically realisable with the specified array geometry.

The algorithm, as described here, is easily implemented as a computer program either in conventional programming languages or the more recent 'mathematical' packages. The examples discussed in [3] were obtained with BASIC programs, those in [4] used Mathcad, whilst the results discussed in this paper were produced using IDL. Compared with earlier numerical approaches (eg [2]) this method is not computer intensive and for the 55 element array considered Eq.(14) was formulated in its 3-dimensional form and solved within seconds on a PC.

These examples do not represent any specific beamforming application, but are intended to show the sort of problems that can be tackled using the least-squares technique, and to demonstrate that reasonable solutions can be obtained quickly and easily. Nevertheless, the method cannot be applied blindly. Care is needed in specifying the desired beampattern. The algorithm does not know anything about this pattern apart from the points supplied. The curve that fits these points is not necessarily unique, and to get the best results the important features such as the main beam, sidelobes and null positions must be identified. It should also be remembered that sidelobes are not necessarily in phase with the main beam and that if symmetry in the pattern or coefficients is wanted it must be specifically defined.

However, if these points are observed and the method is applied intelligently with an understanding of the behaviour of arrays and beamformers, the result is an efficient tool capable

of finding shading coefficients for any arbitrary array geometry and a given set of beampattern requirements.

5. ACKNOWLEDGEMENTS

This work was carried out with the support of the Defence Research Agency.

6. REFERENCES

[1] M H Er, S L Sim and S N Koh, 'Application of Constrained Optimization Techniques to Array Pattern Synthesis', *Signal Processing*, 34(3), 323-334 (1993).

[2] G L Wilson, 'Computer Optimization of Transducer-Array Patterns', *J. Acoust. Soc. Am.*, 59(1), 195-203 (1976).

[3] P F Dobbins, 'How to Find Shading Coefficients that Produce an Arbitrary Beampattern from an Arbitrary Array', *Proc. Inst. Acoust.*, 13(2), 243-250 (1991).

[4] P F Dobbins and G J Heald, 'General Radiation Pattern Synthesis Technique for Sonar Transducer Arrays', *Proc. UDT '94*, Nexus Business Communications 206-210, (1994).

[5] D C Kreider, R G Kuller, D R Ostberg and F W Perkins, *An Introduction to Linear Analysis*, Addison-Wesley (1966).

[6] R J Bobber, *Underwater Acoustic Measurements*, US GPO Catalog D210.2; UN 2/2, p260 (1970).